Long-lived particles from exotic Higgs decays at the FCC-ee - detector comparison and additional Z decay modes

Mark Larson[1], Louise Skinnari[1]

[1]Northeastern University

Email: larson.ma@northeastern.edu, l.skinnari@northeastern.edu

September 25, 2024

Abstract

This note presents work expanding upon the first sensitivity analysis for long-lived scalar particles from exotic Higgs boson decays at the electron-positron stage of the Future Circular Collider (FCC-ee) within the FCCAnalyses framework. The original analysis studies the production of a Higgs boson in association with a Z boson in electron-positron collisions at a center-of-mass energy of 240 GeV, where the Higgs boson decays into two long-lived scalars, each decaying into a bottom anti-bottom quark pair, and the Z boson decays leptonically. Signal points with scalar masses of $m_s = 20$ and 60 GeV are considered, with mixing angles of $\sin(\theta) = 10^{-5}$, 10^{-6}, and 10^{-7}. The original analysis uses a displaced vertex-based event selection, with displaced vertices reconstructed using the FCCAnalyses version of the secondary vertex finding algorithm, LCFIPlus.

We expand upon the original analysis by comparing results obtained using the IDEA and CLD detector designs, providing an assessment of displaced tracking performance with each tracker design. It is found that, particularly for the ≈ 0.3 and 8 m lifetime signal points, sensitivity is lost using the CLD detector, as tracks from the scalar particle decay products are not formed due to a lack of hits or acceptance within the CLD tracker. Separately, analysis strategies incorporating hadronic and invisible Z decays are presented, however, not yet in a final state. To identify the Z boson in each signal, a missing energy cut is used for invisible decays, and a jet energy cut is used for hadronic decays. The original displaced vertex selection is still applied to identify the long-lived scalars. The preliminary results indicate that incorporating additional Z decay modes could greatly expand the signal sensitivity, however, the strategy particularly incorporating hadronic Z decays needs to still be refined to improve background rejection.

1 Introduction

While the Standard Model (SM) has been incredibly successful in making accurate experimental predictions, it does not account for a variety of experimental observations within our universe. Some of these open questions include what is dark matter, how do neutrinos get their masses, and why is there asymmetry between the amount of matter and anti-matter within our universe. Many beyond the Standard Model (BSM) theories have been developed to address these questions. These theories often predict that the Higgs boson may couple to and hence decay into new BSM particles [4]. Additionally, some of these theories predict the existence of long-lived particles (LLPs) or particles with macroscopic mean decay lengths. Long-lived particles present unique and challenging experimental signatures, and hence may have been missed by standard searches at previous colliders that focus on reconstructing prompt decays.

The FCC-ee, in addition to being a high precision tool with its high luminosity, few trigger limitations, and clean experimental environment, would provide powerful opportunities to conduct searches for long-lived particles [13]. Despite the ideal collision environment for searching for long-lived particles, it is nonetheless important to indicate the feasibility of these searches given different detector designs as, for example, the reconstruction of displaced vertices is heavily dependent on the acceptance of the detector's tracking system.

This study and note present an expansion upon a sensitivity study to long-lived particles from exotic Higgs boson decays at the Zh (240 GeV center-of-mass energy) production stage of the FCC-ee described in Ref. [12]. This study and note are split into two parts which will be discussed sequentially. First, in Section 2, a comparison of sensitivity using two of the different proposed detector concepts, IDEA and CLD, is presented, indirectly providing a comparison of displaced tracking using the two different tracker designs. Secondly, in Section 3, analysis strategies to increase signal sensitivity by incorporating additional Z decay modes (invisible and hadronic) are presented. Further motivation and background to this study are presented in the rest of Section 1.

1.1 Theoretical motivation of LLPs from exotic Higgs boson decays

This study uses a Hidden Valley model [9], which could be motivated by explaining the hierarchy problem of the SM by a scalar extension of the SM. In this model the Higgs boson decays to a long-lived scalar particle that serves as a link between the SM and a weakly interacting, or dark, sector, which could potentially explain dark matter. This extension of the SM is achieved by the following addition of a scalar field S to the SM Lagrangian:

$$\mathscr{L}_{\text{SM}} \ni \underbrace{\frac{1}{2}\mu^2 S^2 - \frac{1}{4!}\lambda_s S^4}_{\text{scalar potential}} - \underbrace{\frac{1}{2}\kappa S^2 |H|^2}_{\text{portal term}}. \tag{1}$$

This results in the following partial decay width of the Higgs boson:

$$\Gamma(h \to ss) \approx \frac{\kappa^2 v_h^2}{32\pi m_h}\sqrt{1 - \frac{4m_s^2}{m_h^2}}, \tag{2}$$

where $v_h = 246$ GeV and $m_h = 125$ GeV, and κ is the coupling between the scalar and Higgs boson determining in part the cross section for scalar production, which, based on previously established limits discussed in Ref. [3], is chosen to be 7×10^{-4}.

In this model the scalar decays to a fermion anti-fermion pair, with the decay modes being determined by the following scalar partial decay width:

$$\Gamma(s \to \bar{f}f) \approx \sin^2\theta \, \frac{N_c m_s m_f^2}{8\pi v_h^2} \left(1 - \frac{4m_f^2}{m_s^2}\right)^{3/2}, \tag{3}$$

where m_f is the mass of the decay product fermion, N_c is the number of colors taken by the decay product fermion, and $\sin(\theta)$ is the mixing angle determining the decay rate to SM fermions and hence in part the lifetime of the scalar. For $\sin(\theta) \leq 10^{-6}$ the mean decay length, $c\tau$, becomes macroscopic and hence the scalar particles become long-lived. Equations 1–3 are taken from Ref. [3]. Equation 3 yields the scalar branching ratios shown in Figure 1, which in turn motivate using the $2s \to 4b$ process for the mass points of $m_s = 20$, 60 GeV. So far, a scalar mass range of 30–40 GeV and lifetime range of 0.1 mm–10 m have been probed by the LHC experiments, thus motivating the choice of scalar masses outside this range.

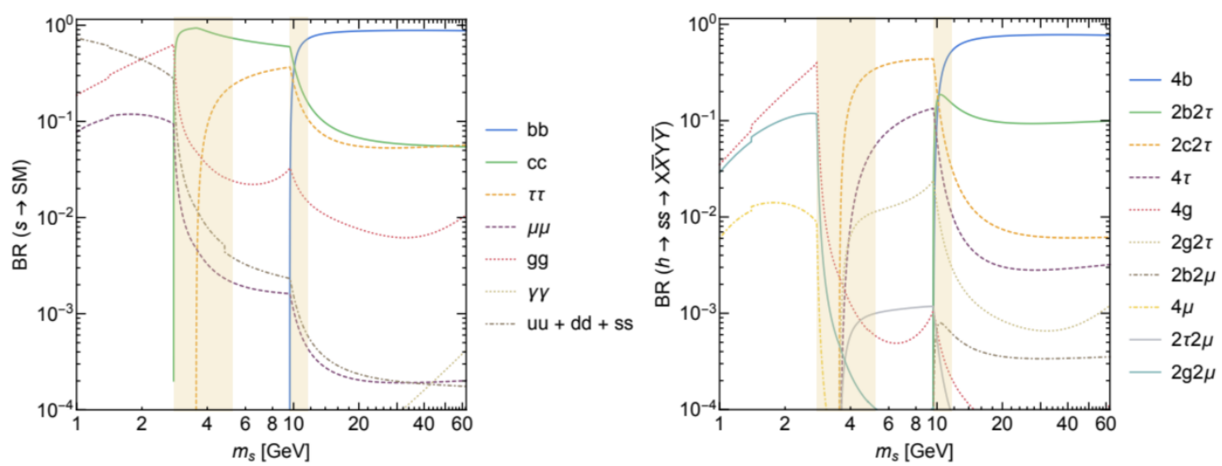

Figure 1: Branching ratios for (left) scalar to SM particles, and (right) the full signal process of a Higgs boson decaying to two scalars to SM particles, taken from Ref. [4].

A more in depth and rigorous discussion of the theoretical motivation, as well as current constraints and possible future sensitivities, is given in Section 2 of the original analysis note [12].

1.2 IDEA and CLD detector concepts

Two baseline detector concepts, designed to meet certain performance requirements such as high $p_T$resolution with a low material budget in the tracker, or high jet energy resolution in the calorimeter, have been primarily used in detailed physics studies for the FCC-ee [6]: the Innovative Detector for e^+e^- Accelerator (IDEA) and the CLIC-like Detector (CLD), which was adapted to the FCC-ee from an International Linear Collider (ILC) detector design. For the purpose of this note, only the differences in the tracker designs, which have the largest effect on sensitivity to long-lived scalars from exotic Higgs decays, will be discussed. However, it is important to note that to measure the scalar mass or incorporate hadronic Z decays to the signal process, differences in the calorimeter may also be of importance. The IDEA detector design is depicted in Figure 2 and the CLD tracker design is depicted in Figure 3.

1.2.1 IDEA tracker

The IDEA tracker is optimized to have a minimal impact on the $p_{\mathrm{T}}$of its tracks due to many tracks at the FCC-ee having low momenta [6]. To accomplish this, the tracker consists of an ultra-light drift chamber, providing coverage from R = 0.35 m to 2 m from the interaction point (IP) with 112 layers, assisted by a silicon pixel vertex detector, providing coverage from R = 1.37 to 31.5 cm with 5 Monolithic Active Pixel Sensors (MAPS) layers. Additionally, the tracker is situated within a ~ 2 T constant magnetic field. Further details of the performance and design of the drift chamber and vertex detector are discussed in Ref. [7].

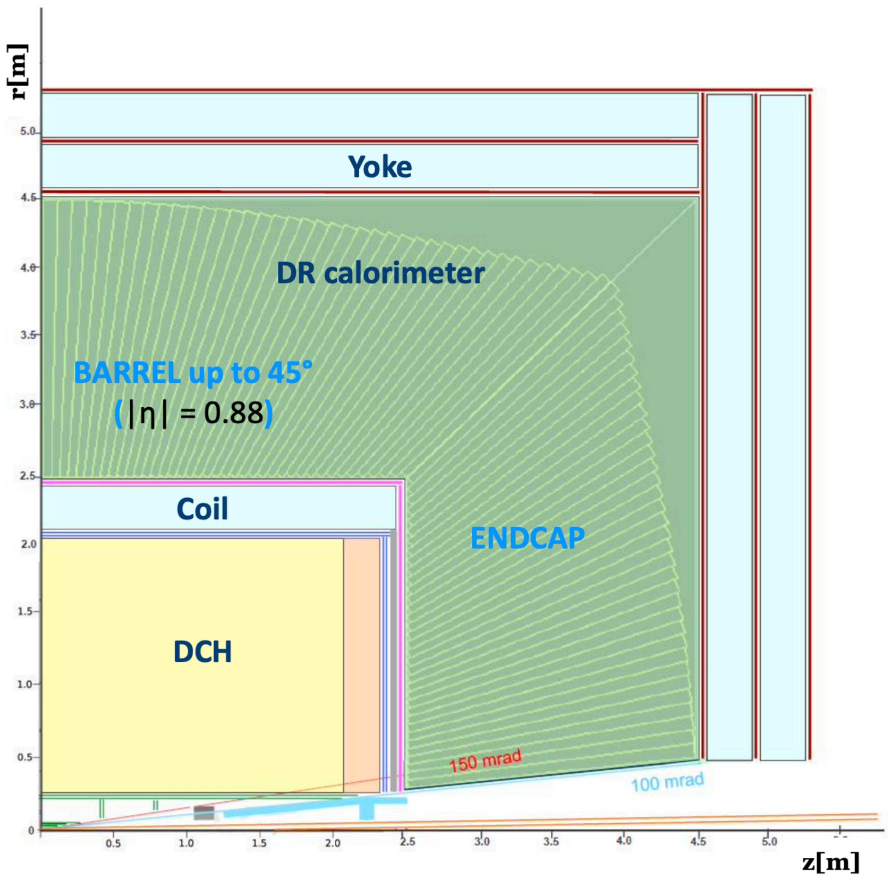

Figure 2: Layout of IDEA detector showing different sub-detectors within the rz-plane. Taken from Ref. [7].

1.2.2 CLD tracker

The CLD tracker consists of a vertex-detector as well as inner and outer trackers consisting of silicon layers. The vertex detector uses doublet layers, and provides coverage up to around R = 13.0 mm. The inner tracker provides coverage up to around R = 0.7 m, and the outer tracker coverage up to around R = 2.1 m. Both the inner and outer tracker consist of 3 layers, along with 7 inner and 4 outer endcap disks.

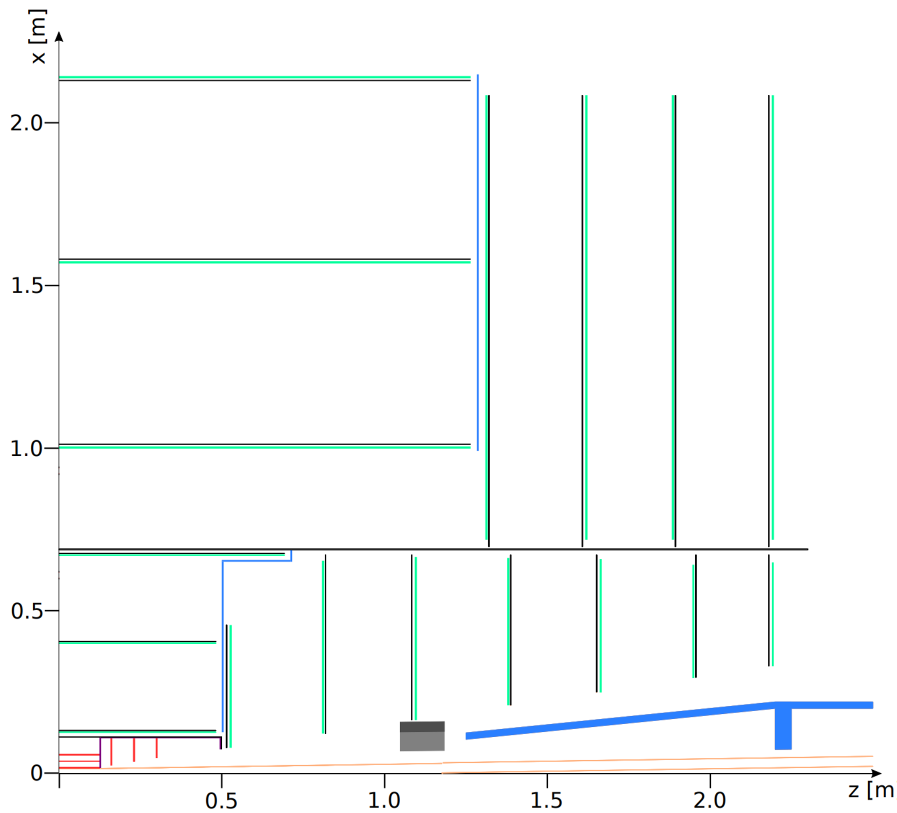

Figure 3: Layout of the CLD tracker showing vertex detector layers in red, and inner and outer tracker layers in light green. Taken from Ref. [8].

Assuming a requirement of at least 4 hits needed to form a track, this results in acceptance for the CLD tracker of up to around decay vertices of $L_{xy} = 0.7$ m for indirect detection of long-lived particles via their decay product tracks (for barrel only tracks), whereas the IDEA tracker, due to its drift chamber consisting of many more layers, would provide coverage nearly to the edge of its tracker around $L_{xy} = 2$ m. This will be more quantitatively illustrated in the results of Section 2. More details about the tracker design and performance are discussed in Ref. [8].

Further details about the IDEA detector and the use of these detector designs within the simulation and software setup is available in Sections 2 and 3 of the original analysis note [12]. This will also be briefly discussed within the context of this study in Sections 2.2 and 3.2.

2 IDEA and CLD detector comparison

This section focuses on the first part of the study, which compares the sensitivity to long-lived scalars from exotic Higgs decays using the IDEA and CLD detector designs. This indirectly provides an evaluation of the prospects of displaced track and vertex reconstruction with each detector design, evaluating how each tracker geometry may affect the ability to indirectly reconstruct long-lived particle signatures by reconstruction of their decay products. This is the first study of its kind comparing sensitivity to long-lived particles between detector concepts for the FCC-ee.

2.1 Signal and background generation

The signal process considered is Zh production at the 240 GeV center-of-mass stage of the FCC-ee, with the Higgs boson decaying into two scalars. Signal events are simulated using files developed for the original analysis. This uses the HAHM MG5Model v3, or the Hidden Abelian Higgs Model, in process cards in MadGraph [1] v.3.4.1. Additionally, Pythia [2] v.8303 is used for parton showering and hadronization. To probe phase space outside of what has already been constrained at the LHC, 6 signal points detailed in Table 1 are used. To simulate and reconstruct these events using the IDEA and CLD detector concepts, Delphes [5] is used with the winter2023 IDEA and CLD cards, whereas the original analysis results presented in Ref. [12] used the spring2021 IDEA card. For each signal point, 10,000 events are generated and reconstructed.

Further details about signal generation and validation is available in Section 6 of Ref. [12].

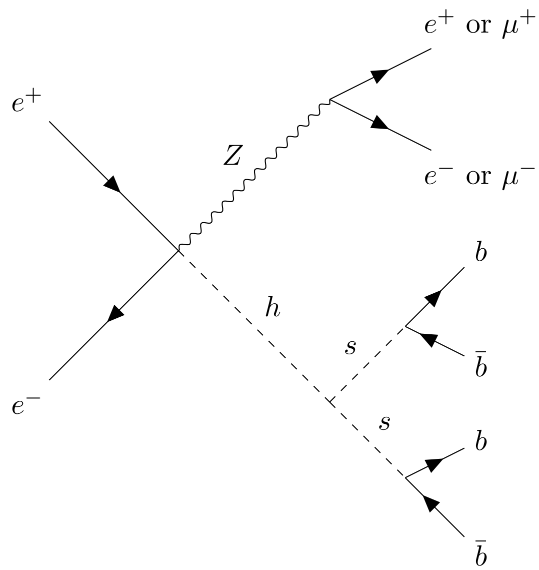

Figure 4: Feynman diagram of the signal process $h \to ss \to b\bar{b}b\bar{b}$ produced at the FCC-ee from $e^+e^- \to Zh$ with the Z boson decaying into e^+e^- or $\mu^+\mu^-$ pairs, used for generation of the IDEA and CLD samples.

Scalar mass m_s [GeV]	Mixing angle $\sin(\theta)$	Mean decay length $c\tau$ [mm]
20	10^{-5}	3.4
20	10^{-6}	341.7
20	10^{-7}	34167.0
60	10^{-5}	0.9
60	10^{-6}	87.7
60	10^{-7}	8769.1

Table 1: Generated values for the scalar mass, m_s, and mixing angle, $\sin\theta$, with corresponding mean proper lifetime, $c\tau$.

In Figure 5, the truth level decay lengths for each signal point are presented. This provides a validation of the expected mean decay lengths for each sample, and their dependence upon the scalar mass and mixing angle. Additionally, one can see the expected levels of acceptance given the tracker designs of IDEA and CLD, which is later verified by the track finding for each signal point.

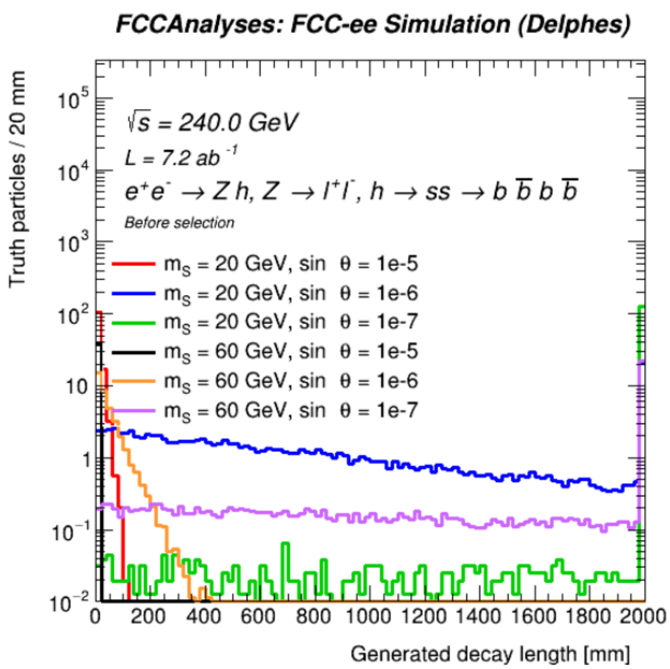

Figure 5: Generated decay length distributions L_{xyz} for each signal point. Taken from [12].

Several SM background processes are considered, including WW, ZZ, and Zh production at $\sqrt{s} =$ 240 GeV. Incorporating the WW process allows for a test of the Z boson tagging method. SM Zh and ZZ production may share similar final states to that of the signal process, particularly with $\ell^+\ell^- + b\bar{b}$ final states, where $\ell = e, \mu$, from $Z, H \to \ell^+\ell^-$or $b\bar{b}$ decay modes. For each background process, 100,000 events of centrally produced background samples, using the spring2021 IDEA card, with inclusive decays for each process, are used. Currently, no centrally produced CLD background samples are available, however, it would be important to verify that similar levels of background rejection are achieved.

2.2 Event processing and reconstruction

Event reconstruction is performed in two main steps. First, the detector response and first level reconstruction, including charged particle track finding, is simulated using the Delphes IDEA or CLD detector cards. Secondly, another pass of reconstruction within the FCCAnalyses framework is performed. In the IDEA and CLD Delphes cards, a minimum number of hits required to accept a track is defined, with a nominal value of 6 hits. This will later be reduced to 5 and 4 to increase the acceptance of scalar decay lengths for the CLD detector in particular. The main difference between the IDEA and CLD detector cards used is in the definition of their tracker geometries, as was detailed in Sections 1.2.1 and 1.2.2, which in turn leads to the differences seen in track reconstruction and later the found sensitivities to the signal process.

In the second reconstruction step using the FCCAnalyses framework, certain variables of interest such as the reconstruction level kinematics of the leptons from the Z boson decay, their reconstructed invariant mass, the number of reconstructed tracks, etc., are selected to be written to a ROOT NTuple file. Additionally, the displaced vertex reconstruction algorithm is run to identify the displaced vertices generated by the scalar decay products.

2.2.1 Reconstruction of displaced vertices

The displaced vertex reconstruction algorithm is based on the secondary vertex finder within the FCCAnalyses framework, which is in turn based on the LCFIPlus vertex finder, detailed in Ref. [10]. To adapt the secondary vertex finder to find particularly displaced vertices that could be used to identify the scalar particles, selections are made upon tracks inputted to the vertex finder. The tracks are required to have $p_{\mathrm{T}} \geq 1$ GeV, and a transverse impact parameter of $|d_0| > 2$ mm. For a more in depth description of the displaced vertexing algorithm, see Section 5 of Ref. [12].

2.3 Event selection

After running the secondary pass of reconstruction within the FCCAnalyses framework, a series of selections are applied to the output ROOT NTuples in an effort to reject SM background processes and identify production of the long-lived scalars. The cut flow used in the original analysis, and identically used in this detector card comparison study, is shown in Table 2. First, a selection upon the number of reconstructed oppositely charged electrons or muons is applied to identify the leptonic decay of the Z boson. Next, a cut on the reconstructed invariant mass of these leptons is applied using a window of ~ 20 GeV around the Z mass to ensure that these leptons indeed come from the decay of the Z boson. Lastly, a cut is applied requiring the number of reconstructed displaced vertices to be ≥ 2.

Selection	**Criteria**
Pre-selection	≥ 2 oppositely charged electrons or muons
Z boson tag	$70 < m_{\ell\ell} < 110$ GeV
Multiplicity of DVs	$n_{\mathrm{DVs}} \geq 2$

Table 2: Summary of selection criteria applied to reconstructed variables, taken from Ref. [12].

2.4 Tracking, vertex finding, and sensitivity results

The initial changes in sensitivity when using the IDEA and CLD detector concepts in Delphes are presented in Tables 3 and 4. The averaged background sensitivities for the spring2021 IDEA centrally produced samples are presented in Table 5, for which the final displaced vertex cut saw complete background rejection. Results for the winter2023 IDEA cards are expected to be similar, however, this, and results using the winter2023 CLD card, should be studied in its own right.

Significant decreases in sensitivity (including a loss of sensitivity using the definition of ≥ 3 events predicted to be observed) were seen for particularly the $m_s = 20$ GeV, $\sin(\theta) = 10^{-6}$ and $m_s = 60$ GeV, $\sin(\theta) = 10^{-7}$ samples, which notably have longer mean decay lengths of 341.7 and 8769.1 mm, respectively.

	20 GeV, 1e-5	20 GeV, 1e-6	20 GeV, 1e-7
Before selection	1.0	1.0	1.0
Pre-selection	0.957	0.950	0.949
$70 < m_{\ell\ell} < 110$ GeV	0.888	0.888	0.900
$N_{\text{DVs}} \geq 2$	0.091	0.672	0.014
	60 GeV, 1e-5	60 GeV, 1e-6	60 GeV, 1e-7
Before selection	1.0	1.0	1.0
Pre-selection	0.957	0.957	0.951
$70 < m_{\ell\ell} < 110$ GeV	0.894	0.895	0.896
$N_{\text{DVs}} \geq 2$	0.0002	0.672	0.398

Table 3: IDEA Samples cut flow showing the efficiencies for each step of event selection applied cumulatively from top down. Each signal point is labelled by [m_s, $\sin(\theta)$].

	20 GeV, 1e-5	20 GeV, 1e-6	20 GeV, 1e-7
Before selection	1.0	1.0	1.0
Pre-selection	0.955	0.952	0.952
$70 < m_{\ell\ell} < 110$ GeV	0.891	0.896	0.903
$N_{\text{DVs}} \geq 2$	0.092	0.109	0.002
	60 GeV, 1e-5	60 GeV, 1e-6	60 GeV, 1e-7
Before selection	1.0	1.0	1.0
Pre-selection	0.958	0.958	0.952
$70 < m_{\ell\ell} < 110$ GeV	0.895	0.897	0.899
$N_{\text{DVs}} \geq 2$	0.0002	0.654	0.0502

Table 4: CLD samples cut flow showing the efficiencies for each step of event selection applied cumulatively from top down. Each signal point is labelled by [m_s, $\sin(\theta)$].

	WW	ZZ	Zh
Pre-sel and $70 < m_{\ell\ell} < 110$	0.006	0.086	0.047
$N_{\text{DVs}} \geq 2$	0.0	0.0	0.0

Table 5: Cut flow showing average efficiencies across WW, ZZ, and Zh spring2021 IDEA backgrounds, taken from Ref. [12].

It was found that for these longer lifetime samples fewer tracks were reconstructed, and thus fewer displaced vertices reconstructed and fewer signal events passed the final cuts. This is illustrated in Figure 6, for which when using the CLD detector concept almost 40% of events saw only the tracks from the leptonic Z decay reconstructed and no displaced tracks from the scalar decay products, whereas this was only the case for around 1% of IDEA events.

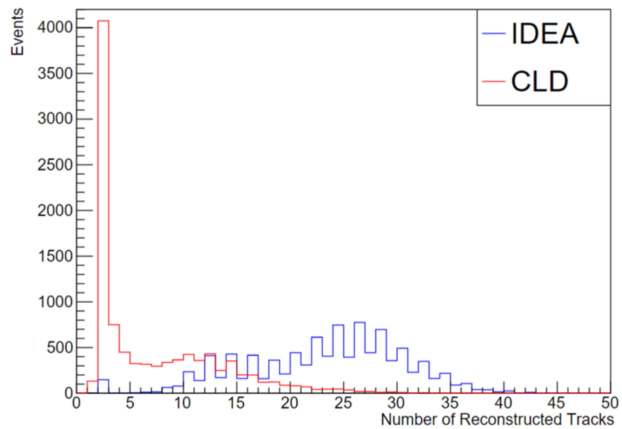

Figure 6: Number of reconstructed tracks per event for the $m_s = 20$ GeV, $\sin(\theta) = 10^{-6}$ sample for which a significant loss in sensitivity was found when using the CLD detector.

To mitigate the loss in acceptance due to the CLD tracker geometry, the minimum required number of hits to accept a track was decreased to 5 and 4, and the resulting sensitivities were examined. The changes in sensitivity for the IDEA samples, and the CLD samples for each minimum hit requirement, are presented in Table 6. The efficiencies for the two longer lifetime CLD samples significantly increased, up to a factor of 4, however, still did not recover to the levels of efficiency of the IDEA samples. For the shorter lifetime CLD samples, efficiency levels notably slightly increased to be slightly higher than those of the IDEA samples.

m_s [GeV], $\sin(\theta)$	IDEA	CLD ($\geq$ 6 hits)	CLD ($\geq$ 5 hits)	CLD ($\geq$ 4 hits)
20, 10^{-5}	0.091	0.092	0.094	0.096
20, 10^{-6}	0.672	0.109	0.293	0.441
20, 10^{-7}	0.014	0.002	0.0042	0.0056
60, 10^{-5}	0.0002	0.0002	0.0003	0.0002
60, 10^{-6}	0.672	0.654	0.684	0.687
60, 10^{-7}	0.398	0.0502	0.123	0.183

Table 6: Final selection efficiencies for all IDEA and CLD samples, including comparing samples using different requirements on the minimum number of hits to form tracks for the CLD samples.

The results of the number of hits used to form tracks (and their x-coordinate distribution), the number of tracks reconstructed per event, and the number of displaced vertices reconstructed per event for a shorter lifetime sample ($m_s = 60$ GeV, $\sin(\theta) = 10^{-6}$) and a longer lifetime sample ($m_s = 20$ GeV, $\sin(\theta) = 10^{-6}$) are presented in Figures 7 and 8, respectively. Here it is seen that reducing the minimum hit requirement is especially helpful for the longer mean decay length sample, with only negligible improvements in the number of tracks and displaced vertices reconstructed for the shorter lifetime sample, but significant improvement for the longer lifetime sample.

Legend (Fig. 7 a-c): Min. 4 hits   Min. 5 hits   Min. 6 hits

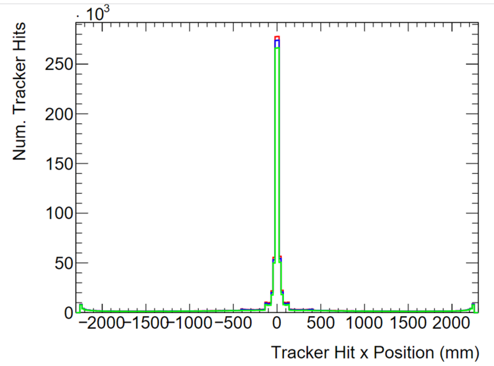

(a) Distribution of hits used to form tracks when modifying the minimum hit requirement.

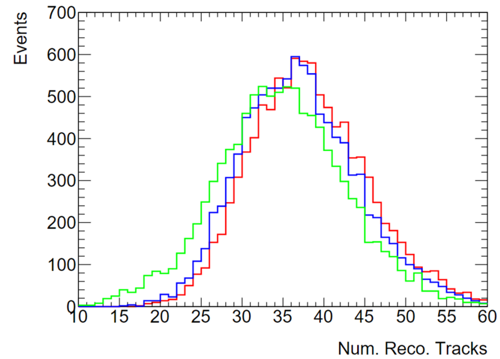

(b) Number of tracks reconstructed per event when modifying the minimum hit requirement.

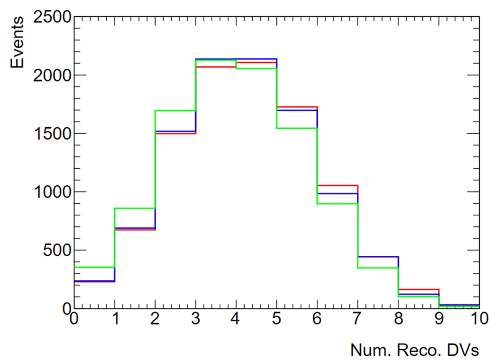

(c) Number of displaced vertices reconstructed when modifying the minimum hit requirement.

Figure 7: Tracking and vertex finding results when modifying the minimum number of hits required to accept tracks, shown for the $m_s = 60$ GeV, $\sin(\theta) = 10^{-6}$ ($c\tau = 87.7$ mm) signal sample (10,000 events) and the CLD tracker detector.

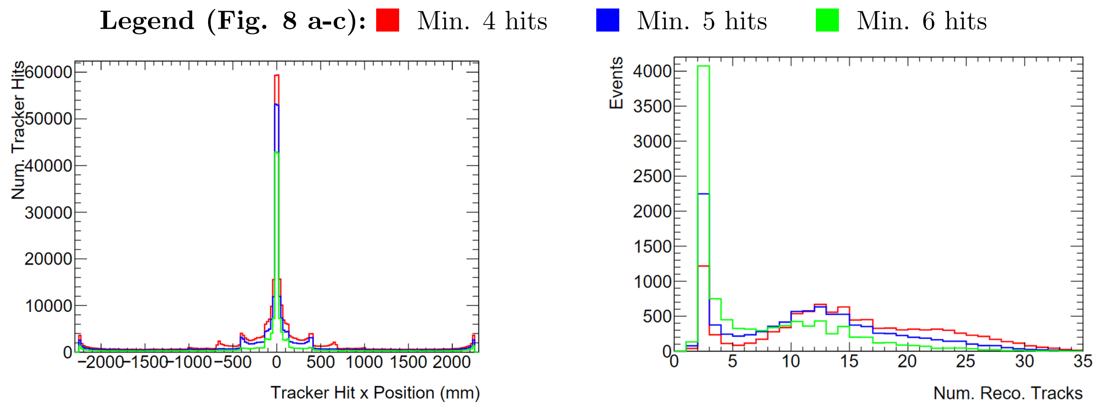

(a) Distribution of hits used to form tracks when modifying the minimum hit requirement.

(b) Number of tracks reconstructed when modifying the minimum hit requirement.

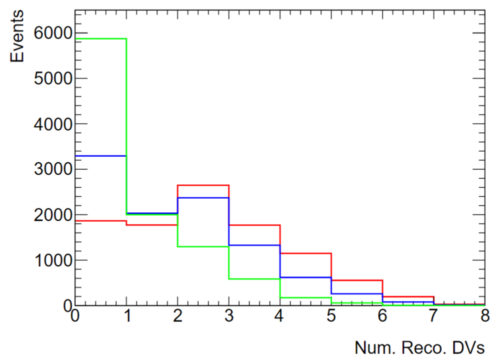

(c) Number of displaced vertices reconstructed when modifying the minimum hit requirement.

Figure 8: Tracking and vertex finding results when modifying the minimum number of hits required to accept tracks, shown for the $m_s = 20$ GeV, $\sin(\theta) = 10^{-6}$ ($c\tau = 341.7$ mm) signal sample (10,000 events) and the CLD tracker detector.

Lastly, the expected number of observed signal and background events at the 240 GeV center-of-mass stage of the FCC-ee based on an integrated luminosity of 7.2 ab^{-1} are presented, respectively, in Tables 7 and 8.

To obtain the number of expected signal events given our efficiencies, we first convert from the number of generated events to the number of expected selected events given the total 1.45×10^6 number of scaled Zh events (corresponding to an integrated luminosity of 7.2 ab^{-1}), using Equation 4:

$$N_{\text{tot}} = N_{Zh} \times \text{BR}(Z \to \ell^+\ell^-) \times \text{BR}(h \to ss \to b\bar{b}b\bar{b}). \tag{4}$$

The number of expected background events can be obtained by multiplying the cross section by the integrated luminosity of 7.2 ab^{-1}. With the total expected events, one can convert to the number of expected selected events by multiplying the selection efficiency times the total expected events. For $m_s = 20$ GeV, there were 55.20 total expected events, and for $m_s = 60$ GeV, there were 16.32 total expected events. The uncertainty in the number of expected selected events are calculated using:

$$\sigma_{\text{error}} = \frac{N_{\text{tot}}}{N_{\text{tot}}^{\text{gen}}} \sqrt{N_{\text{cut}}^{\text{gen}}}. \tag{5}$$

m_s [GeV], $\sin(\theta)$	IDEA	CLD (min. hits = 6)	CLD (min. hits = 5)	CLD (min. hits = 4)
20, 10^{-5}	5.02 ± 0.17	5.08 ± 0.17	5.19 ± 0.17	5.30 ± 0.17
20, 10^{-6}	37.1 ± 0.45	6.02 ± 0.18	16.17 ± 0.30	24.34 ± 0.37
20, 10^{-7}	0.77 ± 0.07	0.11 ± 0.02	0.23 ± 0.04	0.31 ± 0.04
60, 10^{-5}	0.003 ± 0.002	0.003 ± 0.002	0.006 ± 0.005	0.003 ± 0.002
60, 10^{-6}	10.97 ± 0.13	10.67 ± 0.13	11.16 ± 0.13	11.21 ± 0.14
60, 10^{-7}	6.50 ± 0.10	0.82 ± 0.04	2.01 ± 0.057	2.99 ± 0.07

Table 7: Expected signal events after all selections are applied for all IDEA and CLD samples with statistical uncertainties.

Background process	IDEA (spring2021)
WW	0 ($\leq 2.90 \times 10^4$)
ZZ	0 ($\leq 9.34 \times 10^3$)
Zh	0 ($\leq 1.03 \times 10^3$)

Table 8: Expected IDEA background events after all selections with statistical uncertainties. The constraint on the number of expected events for fully rejected background samples is taken to be equal to uncertainty of the previous cut level.

Given the results in Tables 7 and 8, we see that using the baseline CLD Delphes detector card, based on the definition of sensitivity as expecting ≥ 3 events, we lose sensitivity to the $m_s = 60$ GeV, $\sin(\theta) = 10^{-7}$ ($c\tau \sim 8.7$ m) sample. Additionally, the number of expected events is greatly decreased for the $m_s = 20$ GeV, $\sin(\theta) = 10^{-7}$ ($c\tau \sim 341.7$ mm) sample. However, reducing the minimum number of hits required to form a track to 4 increases the expected number of events by around a factor of 4 for these samples, and minimally for other sensitive samples, nearly regaining sensitivity for the $m_s = 60$ GeV, $\sin(\theta) = 10^{-7}$ sample. For the spring2021 IDEA detector backgrounds, we see a relatively weak statistical constraint on the number of expected background events due to a low number of background events generated (100,000). Background efficiencies and constraints have yet to be studied for the winter2023 IDEA centrally produced backgrounds or the winter2023 CLD card (due to no centrally produced backgrounds being available).

3 Incorporating additional Z boson decay modes

This section details analysis strategies for adding invisible and hadronic decay modes of the signal Z boson. Sensitivities for the original analysis are limited by the branching ratio:

$$\frac{\Gamma(Z \to e^+e^- \text{ or } \mu^+\mu^-)}{\Gamma_Z} \approx 6.72\%,$$

whereas incorporating invisible and hadronic decays would increase the accessible branching fraction to:

$$\frac{\Gamma(Z \to \nu\bar{\nu}\,\mathrm{or}\,q\bar{q})}{\Gamma_Z} \approx 89.11\%,$$

where $\nu = \nu_e, \nu_\mu, \nu_\tau$, and $q = u, d, c, s, b$ [11]. This significant increase in potentially accessible signal events could provide sensitivity for in particular shorter or longer lifetime samples in which either the scalar decays are not displaced enough to pass displaced vertex cuts, or decays are happening mostly outside of the tracker volume. This could therefore increase the phase space that could be constrained at the FCC-ee. However, especially for the hadronic Z decays, it becomes significantly more difficult to differentiate the signal from SM background processes.

This section first details an analysis strategy for including invisible decays of the Z boson as a part of the signal process. This analysis strategy relies on using the same displaced vertex reconstruction and selection as the original analysis to identify the long-lived scalars, however, now uses missing energy, rather than invariant lepton mass, to reconstruct the Z boson. Next, a preliminary analysis strategy for incorporating hadronic decays of the Z boson within the signal process is presented. Again this strategy relies primarily on displaced vertex reconstruction and selection, but now uses the total reconstructed jet energy in the event to identify the Z boson in the process. This will need to be refined to further reject background while maintaining a high signal efficiency.

3.1 Signal and background generation

The same methods used in Section 2.1 were similarly used here to generate new signal samples with the updated Z decay modes. Specifically, only the decay of the Z boson was redefined within the MadGraph process card. The updated signal processes are presented in Figures 9a and 9b. To simulate and reconstruct these events, Delphes is used with the winter2023 IDEA detector card. While these studies could be repeated with CLD, the only difference with the detector card was the tracker geometry, which should only affect the displaced vertex selection for these new analysis strategies. The same 6 signal points are used here, with 10,000 events again generated for each.

The SM backgrounds considered for our signal with additional Z decay modes are again WW, ZZ, and Zh processes, however, the Zh samples are now split by their decay modes to contain similar final states. Again the inclusion of the WW background serves to validate the method of identifying the Z boson in our signal, and the ZZ and Zh processes are expected to have similar final states to our signal. In particular, Zh processes with $Z \to \nu\nu$ and $h \to WW, b\bar{b}$ decay modes are considered as backgrounds for the signal with invisible Z decays, and Zh processes with $Z \to q\bar{q}$ and $h \to WW, b\bar{b}$ are considered as backgrounds for the signal with hadronic Z decays. For each background, 100,000 events of larger centrally produced backgrounds are processed. In the future, including additional Zh processes with additional Higgs boson decay modes and other SM processes with similar final states could be useful in validating the SM background rejection of the presented analysis strategies.

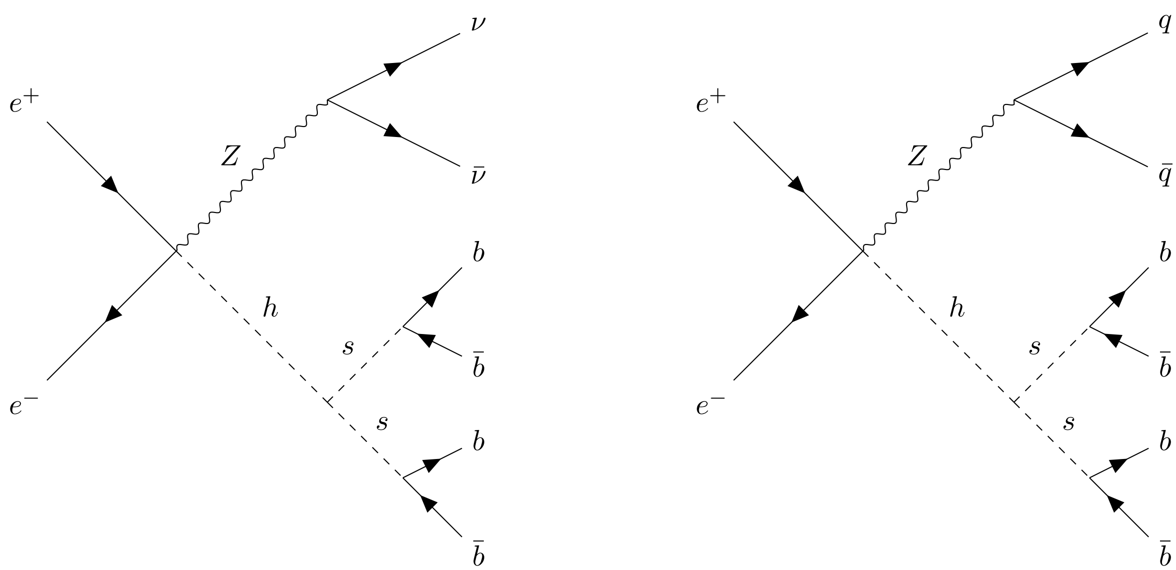

(a) Feynman diagram of the Zh signal process with $h \to ss \to b\bar{b}b\bar{b}$ and the Z boson decaying into $\nu\bar{\nu}$ pairs.

(b) Feynman diagram of the Zh signal process $h \to ss \to b\bar{b}b\bar{b}$ and the Z boson decaying into $q\bar{q}$ pairs, where $q = u, d, c, s, b$.

Figure 9: Feynman diagrams for added decay modes of Z boson

3.2 Event processing and reconstruction

For the purposes of both the addition of invisible and hadronic Z decays, the displaced vertex reconstruction algorithm is left unchanged, and for the addition of invisible Z decays, the entire reconstruction process is left unchanged to the original analysis. For the addition of hadronic Z decays, however, a modification to the existing jet clustering algorithm was necessary.

3.2.1 Jet clustering algorithm

For the purposes of identifying the Z boson through its hadronic decays, obtaining accurately clustered jets, with the correct number of jets per event and accurately reconstructed energy, is important. Due to issues with using standard jet clustering methods available either through Delphes or in the FCCAnalyses framework, a novel strategy was used which is detailed below:

1. Perform displaced vertex reconstruction, as described in Section 2.2.1
2. Duplicate the original complete Monte Carlo particle collection, and remove all particles associated to any track associated to reconstructed displaced vertices.
3. Perform jet clustering in the FCCAnalyses framework with this new particle collection using exclusive $N_{jets} = 2$, k_t, $R_{jets} = 0.5$, energy recombination scheme, jet clustering algorithm.
4. Repeat identically for both signal and backgrounds for consistency.

The jet energy and momentum is then extracted for each reconstructed jet, and for the purpose of a later described selection, summed for each event.

3.3 Event selection

3.3.1 Invisible Z decays

For the addition of invisible Z decays to the signal process, the previously used pre-selection and lepton invariant mass selections are replaced with a looser, yet analogous, selection, now on the missing energy per event. This selection is based off of a peak of reconstructed missing energy between 45–55 GeV due to the neutrinos from the Z decay not being reconstructed. It is important to better understand the shape and value of the peak of the distribution, but this will be left for a future study. The updated selections are shown in Table 9, and results showing the missing energy distribution after all selections are shown in Figure 10.

Selection	**Criteria**
$E_{missing}$	$30 < E_{missing} < 70$ GeV
Multiplicity of DVs	$n_{\text{DVs}} \geq 2$

Table 9: Summary of selection criteria applied to invisible Z decay signals and backgrounds.

3.3.2 Hadronic Z decays

For the addition of hadronic Z decays to the signal process, the previously used pre-selection and lepton invariant mass selections are again replaced with a looser, yet analogous, selection now on the total reconstructed jet energy (using jets reconstructed from the modified clustering algorithm). For the purpose of illustrating the maximum possible signal sensitivity gained, only a very loose selection has been applied so far, as likely a tighter total jet energy (or different altogether) selection will be necessary to improve background rejection. An additional selection could be done either on the available reconstructed variables, or alternatively on the properties of the reconstructed displaced vertices to improve the background rejection on the multiplicity of displaced vertices cut. The total reconstructed jet energy is selected to be between 50 and 140 GeV, based on peaks for signal points being slightly greater than the Z mass, around 95–105 GeV. Additional options will be later discussed in Sections 3.4.2 and 5. The updated selections are shown in Table 10, and results showing the jet energy distribution after all selections are shown in Figure 12.

Selection	**Criteria**
ΣE_{jets}	$50 < \Sigma E_{jets} < 140$ GeV
Multiplicity of DVs	$n_{\text{DVs}} \geq 2$

Table 10: Summary of selection criteria applied to hadronic Z decay signals and backgrounds.

3.4 Preliminary results

Preliminary sensitivity results for the analysis strategies for adding invisible and hadronic Z decays to the signal process are presented in this section. To calculate the number of expected signal events for the changed Z decay modes, the ratio of:

$$\frac{\Gamma(Z \to \nu\bar{\nu} \text{ or } q\bar{q})}{\Gamma(Z \to e^+e^- \text{ or } \mu^+\mu^-)}$$

is multiplied by the previously calculated total number of signal events from Section 2.4, and then multiplied by the calculated efficiencies. The same methods for calculating statistical uncertainties as used in Section 2.4 are used.

3.4.1 Invisible Z decays

The signal acceptance efficiencies after applying the missing energy and displaced vertex selections are shown in Table 11. Very high efficiencies are maintained for all but the longest lifetime samples. This is primarily a result of increased missing energy due to scalar particles decaying outside the detector volume, and hence one would not expect to be able to reconstruct these events anyways. Final signal selection efficiencies are comparable or worse than those of the original leptonic decay analysis, with improvements or the same results for all except the m_s = 60 GeV, $\sin(\theta) = 10^-7$, which saw a roughly 12% decrease in efficiency. The background acceptance efficiencies after applying selections are shown in Table 12. The final displaced vertex selection again achieves full background rejection, with the exception of 1 of 100,000 events for the Zh (Z $\rightarrow \nu\bar{\nu}$, H $\rightarrow$ WW) background.

m_s [GeV], $\sin(\theta)$	20, 10^{-5}	20, 10^{-6}	20, 10^{-7}	60, 10^{-5}	60, 10^{-6}	60, 10^{-7}
$E_{missing}$	0.968	0.939	0.038	0.980	0.981	0.441
$N_{\mathrm{DVs}} \geq 2$	0.102	0.715	0.014	0.0002	0.732	0.276

Table 11: Final selection efficiencies for all invisible Z decay signal points

	WW	ZZ	Zh (Z $\rightarrow \nu\bar{\nu}$, h $\rightarrow$ bb)	Zh (Z $\rightarrow \nu\bar{\nu}$, h $\rightarrow$ WW)
$E_{missing}$	0.158	0.327	0.910	0.822
$N_{\mathrm{DVs}} \geq 2$	0.0	0.0	0.0	0.00001

Table 12: Final selection efficiencies for all invisible Z decay backgrounds, with Zh backgrounds split into separate Higgs boson decay modes.

In Figure 10, the missing energy distributions of signals and the concatenated Zh background are presented, indicating how a significantly tighter cut could reject the final passed Zh event, however, this would be at great detriment to the signal efficiency. In Figure 11 the distribution of the number of reconstructed displaced vertices is presented, indicating the potential to tighten the multiplicity of the DVs selection to $N_{\mathrm{DVs}} \geq 3$ without losing significant signal sensitivity. The higher multiplicity of displaced vertices for signal processes is likely because the b quark scalar decay products travel far enough before decaying to form multiple vertices from one scalar decay. Additionally, one could cut on the number of tracks associated to displaced vertices, which is also significantly lower for the one background event that passed selections. Overall, it is important to repeat these studies with > 100,000 background events to indicate if tighter selections need to be made.

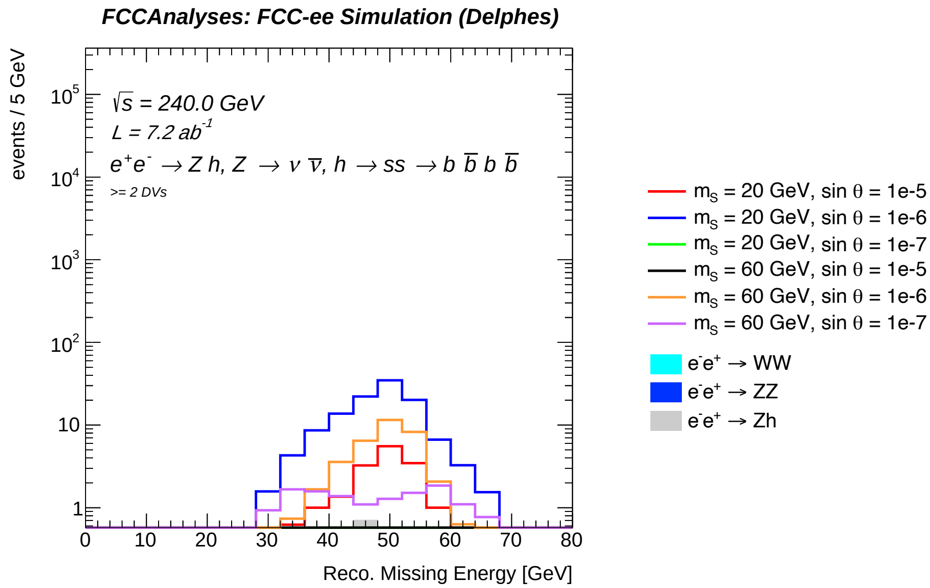

Figure 10: Missing energy distributions for the different signal points and background processes after all selections are applied, with events re-scaled to an integrated luminosity of 7.2 ab^{-1}. Note that the Zh process here is restricted to only the $Z \to \nu\bar{\nu}$ and $h \to$ WW, $b\bar{b}$ decay modes.

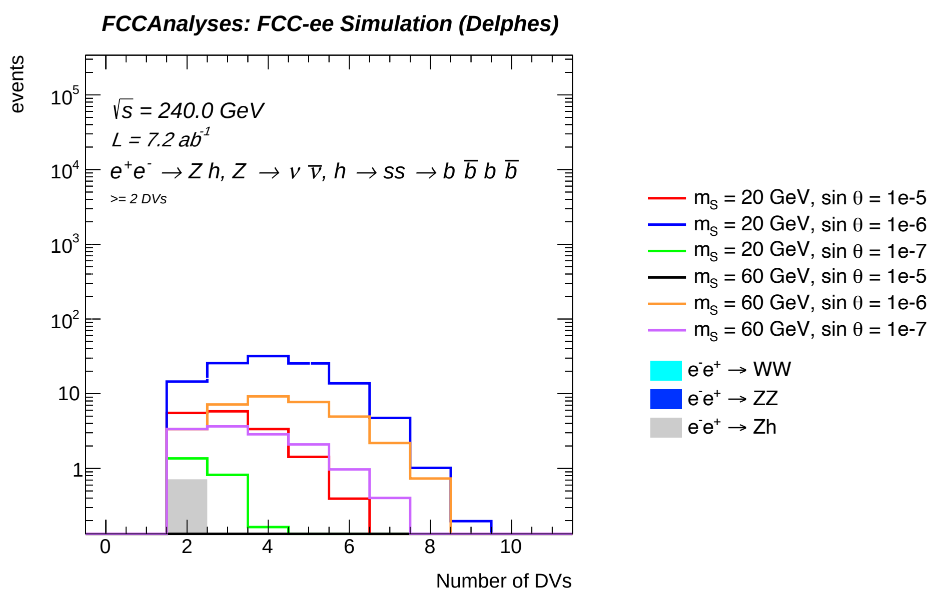

Figure 11: Distribution of the displaced vertex multiplicity for signals and backgrounds after all selections, with events re-scaled to an integrated luminosity of 7.2 ab^{-1}. Note that the Zh process is here restricted to only the $Z \to \nu\bar{\nu}$ and $h \to$ WW, $b\bar{b}$ decay modes.

In Tables 13 and 14 the expected number of signal and background events, respectively, after all selections are presented. As signal efficiencies remain around the same, and the cross section for this signal process is increased by around 3 times, we see around a factor of 3 increase in the expected number of signal events, while maintaining similar statistical constraints on our expected number of background events. Including these results with those of the leptonic analysis would additionally result in gaining sensitivity to the $m_s = 20$ GeV, $\sin(\theta) = 10^{-7}$ signal point. Additionally, there is the potential to use tighter cuts if when repeated with more background events background acceptance becomes an issue as given the higher cross section there is a higher baseline signal sensitivity.

20 GeV, 10^{-5}	20 GeV, 10^{-6}	20 GeV, 10^{-7}	60 GeV, 10^{-5}	60 GeV, 10^{-6}	60 GeV, 10^{-7}
16.73 ± 0.52	117.33 ± 1.39	2.35 ± 0.19	0.01 ± 0.007	35.52 ± 0.41	13.43 ± 0.25

Table 13: Expected signal events, with signal points labelled by m_s [GeV], $\sin(\theta)$, after all selections are applied with statistical uncertainties.

WW	ZZ	Zh ($Z \to \nu\bar{\nu}$, $h \to WW$)	Zh ($Z \to \nu\bar{\nu}$, $h \to bb$)
0 ($\leq 1.49 \times 10^5$)	0 ($\leq 9.8 \times 10^6$)	0 ($\leq 2.16 \times 10^2$)	0 ($\leq 0.72 + 5.8 \times 10^2$)

Table 14: Expected background events after all selections applied with statistical uncertainties.

3.4.2 Hadronic Z decays

The signal acceptance efficiencies are shown in Table 15 after applying the total reconstructed jet energy and displaced vertices selections. Similarly to for the invisible Z decays selections, efficiencies with respect to the original analysis are largely maintained or improved, however, this currently comes at the cost of poor background rejection, as shown in Table 16, in which the different included Zh decay modes are concatenated to yield one efficiency value. Rather than presenting the very low background acceptance numbers (which are on the order of 10−5), the number of events are presented for the final displaced vertex selection to illustrate the necessary improvement. Here we see, as somewhat expected given the very loose cut on total reconstructed jet energy, very poor initial background rejection, especially for Zh events, with the majority of rejection coming from the displaced vertices selection. Background statistical constraints are not calculated here, however, will be very high given the high background acceptance for the jet energy cut, and processing only 100,000 background events for each sample.

	20, 10^{-5}	20, 10^{-6}	20, 10^{-7}	60, 10^{-5}	60, 10^{-6}	60, 10^{-7}
ΣE_{jets}	0.865	0.971	0.964	0.971	0.978	0.967
$N_{\mathrm{DVs}} \geq 2$	0.096	0.735	0.018	0.0002	0.726	0.425

Table 15: Final selection efficiencies for all hadronic Z decay signals with signal points labelled by m_s [GeV], $\sin(\theta)$.

	WW	ZZ	Zh
ΣE_{jets}	0.587	0.683	0.893
$N_{DVs} \geq 2$	1183.6 ev.	97.8 ev.	27.5 ev.

Table 16: Final selection efficiencies and expected events for all hadronic Z decay backgrounds, with Zh backgrounds with different decay modes concatenated into one value.

The expected signal event yields after all selections are shown in Table 17, in which it is shown that, as expected given the increased cross section, around 10 times improvement in signal yield is possible, including gaining sensitivity to the $m_s = 20$ GeV, $\sin(\theta) = 10^{-7}$ signal point, for which most of the scalar particles are decaying outside the tracker. However, an improved analysis strategy must still be developed to retain this level of high signal efficiency while rejecting more background events.

20 GeV, 10^{-5}	20 GeV, 10^{-6}	20 GeV, 10^{-7}	60 GeV, 10^{-5}	60 GeV, 10^{-6}	60 GeV, 10^{-7}
54.86 ± 1.66	421.25 ± 4.60	10.32 ± 0.72	0.033 ± 0.023	123.0 ± 1.43	72.03 ± 1.09

Table 17: Expected number of signal events, with signal points labelled by m_s [GeV], $\sin(\theta)$, after all selections applied with statistical uncertainties.

In Figures 12 and 13 the distributions of reconstructed jet energy and the multiplicity of displaced vertices (the two selected on variables) are shown. While there is significant overlap between the signal and the remaining background events, there is potential to increase the minimum number of displaced vertices to reject a significant portion of the background events while maintaining high signal efficiency, due to the higher signal cross section than, for example, the leptonic Z decay mode signal. Additionally, there is potential cuts within variables related to the reconstructed displaced vertices, such as how many tracks are related to each vertex, and the distance between the primary and secondary vertex, that could also potentially reject the remaining background events.

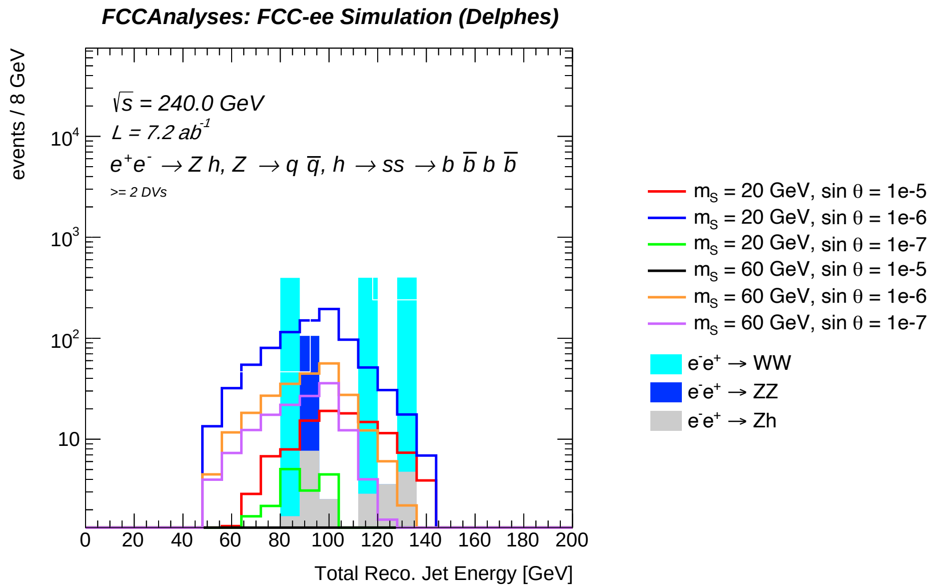

Figure 12: Reconstructed jet energy distributions of signals, background after all selections, with events re-scaled to an integrated luminosity of 7.2 ab^{-1}. Note that Zh process here restricted to only $Z \to q\bar{q}$ and $h \to$ WW, $b\bar{b}$ decay modes.

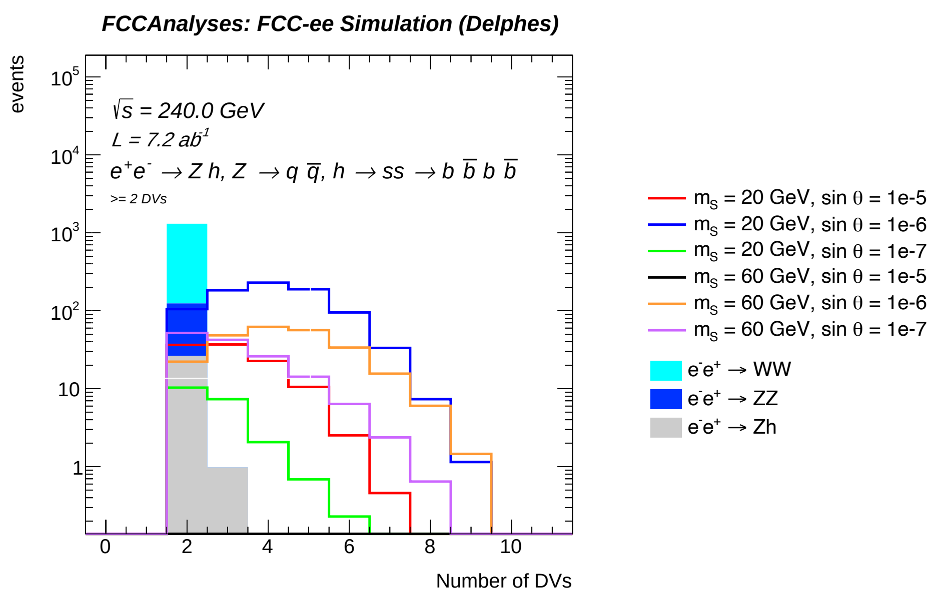

Figure 13: Distribution of displaced vertex multiplicity of signals, background after all selections, with events re-scaled to an integrated luminosity of 7.2 ab^{-1}. Note that Zh process here restricted to only $Z \to q\bar{q}$ and $h \to$ WW, $b\bar{b}$ decay modes.

4 Outlook

Two main broad suggestions can be applied to every portion of the study, which is to consider more signal points, and additional potential SM backgrounds while processing larger event samples. As shown by the relatively high signal efficiency for long mean decay length samples, especially using the IDEA detector concept, probing a wider range of masses and mixing angles could prove useful in indicating a broader range of sensitivity that the FCC-ee may have to such long-lived scalars from exotic Higgs decays. However, the primary constraint of the power of this study still lies in high background uncertainties, and, for the case of the added invisible and hadronic Z decay samples, additional SM backgrounds with similar states not yet probed (such as alternative Higgs boson decay modes for Zh events). Thus, it is important to take full advantage of the FCC-ee winter2023 IDEA centrally produced backgrounds, which could allow a huge reduction in background uncertainty and the ability to explore additional SM backgrounds.

More specific suggestions to each portion of the study are given below.

4.1 Detector sensitivity comparison

While the detector sensitivity comparison between IDEA and CLD has yielded clear results regarding the decreased acceptance for long-lived particle displaced track signatures with the CLD tracker geometry relative to IDEA, there are still many important avenues for expansion of this study. Firstly, the updated winter2023 IDEA backgrounds (and hopefully in the future CLD centrally produced background samples) should be processed with the leptonic Z decay selections to ensure there is still complete background rejection, or if the existing selections need to be altered. Additionally, an examination more directly of the displaced tracking efficiency through, for example, the Delphes validation tool set, could provide a more direct indication of the acceptance ranges for displaced tracks within CLD and IDEA, rather than indirectly relying on the reconstruction of displaced vertices. Particularly examining the displaced tracking efficiency as a function of the minimum hit requirement for CLD samples could provide important insight. Examining distributions of the number of hits per track using IDEA and CLD signal points would also provide a more direct indication of the effect of reducing the minimum hit requirement. Additionally, while this is likely less of a concern given the clean collision environment at the FCC-ee, it is important to investigate whether the rate of fake tracks increases given this reduction in the minimum hit requirement. Finally, it would be helpful to investigate whether any alterations to the displaced vertexing algorithm could be made to accommodate tracks formed in the CLD detector, and its decreased acceptance.

4.2 Adding invisible Z decays

Beyond increasing the background statistics and diversity of SM backgrounds studied, it could be valuable to look into alternative selections either instead of or beyond the existing missing energy cut. In the end, however, it is imperative to repeat these studies using more background events to see how these selections would need to form, and to gain a better understanding for the sensitivity that could be gained by searching for this additional signal process.

4.3 Adding hadronic Z decays

Similarly to the case of adding invisible Z decays, while there is a path forward to rejecting the remaining background events that passed the current selection, it is more important to repeat these studies with more (and again more varied) background events to gain a better understanding of how the current selections would need to be tightened or changed.

5 Conclusions

This study aimed to expand upon the work and existing analysis framework for studying sensitivity to long-lived scalar particles from exotic Higgs boson decays at the FCC-ee through two main goals: investigating the difference in sensitivity using the IDEA and CLD detector concepts, and studying the feasibility of incorporating additional Z decay modes to the signal process.

To accomplish these goals, MadGraph and Pythia were used with the HAHM MadGraph model to generate signal samples with multiple masses and lifetimes corresponding to the 240 GeV center-of-mass energy stage of the FCC-ee, with the Higgs boson decaying to a pair of long-lived scalar particles, each then decaying to a pair of b quarks, and the Z boson decaying leptonically, invisibly, or hadronically. These events were then simulated and reconstructed within the IDEA or CLD detector concepts using DELPHES and FCCAnalyses. A displaced vertexing algorithm based on the secondary vertex algorithm LCFIPlus was used within FCCAnalyses to reconstruct the displaced vertices corresponding to the long-lived scalar particles. Event selections were developed to identify the associated Z boson and the decay products of the long-lived scalar, and separate the signal events from the comparatively high cross section SM backgrounds.

The first goal was largely accomplished, with clear differences in sensitivity to displaced track long-lived particle signatures established and quantified between the IDEA and CLD detector concepts. Particularly, signal points with $c\tau > 300$ mm saw significant decreases in sensitivity. Furthermore, a way to partially mitigate this difference by reducing the minimum hit requirement to form a track for the CLD detector was studied and shown to increase sensitivity especially to longer lifetime samples.

The second goal was partially accomplished, with preliminary analysis strategies to incorporate invisible and hadronic Z decays to the signal process established, indicating the potential to increase the signal yield by up to ~ 13 times. In this, methods to identify the Z boson in our signal, using missing energy and reconstructed jet energy from uniquely clustered jets, were developed. However, further improvements to each analysis strategy must still be made in order to reach the same levels of background rejection as the original leptonic Z decay analysis and demonstrate sensitivity to these signal processes with alternative Z decay modes.

References

[1] Johan Alwall, Rikkert Frederix, Stefano Frixione, et al. The automated computation of tree-level and next-to-leading order differential cross sections, and their matching to parton shower simulations. *Journal of High Energy Physics*, 2014(7):79, 2014. doi: 10.1007/JHEP07(2014)079. URL https://doi.org/10.1007/JHEP07(2014)079.

[2] Christian Bierlich, Smita Chakraborty, Nishita Desai, Leif Gellersen, Ilkka Helenius, Philip Ilten, Leif Lönnblad, Stephen Mrenna, Stefan Prestel, Christian T. Preuss, Torbjörn Sjöstrand, Peter Skands, Marius Utheim, and Rob Verheyen. A comprehensive guide to the physics and usage of pythia 8.3, 2022. URL https://arxiv.org/abs/2203.11601.

[3] María Cepeda, Stefania Gori, Verena Ingrid Martinez Outschoorn, and Jessie Shelton. Exotic higgs decays. *Annual Review of Nuclear and Particle Science*, 72

(Volume 72, 2022):119–149, 2022. ISSN 1545-4134. doi: https://doi.org/10.1146/annurev-nucl-102319-024147. URL https://www.annualreviews.org/content/journals/10.1146/annurev-nucl-102319-024147.

[4] David Curtin, Rouven Essig, Stefania Gori, Prerit Jaiswal, Andrey Katz, Tao Liu, Zhen Liu, David McKeen, Jessie Shelton, Matthew Strassler, Ze'ev Surujon, Brock Tweedie, and Yi-Ming Zhong. Exotic decays of the 125 gev higgs boson. *Phys. Rev. D*, 90:075004, Oct 2014. doi: 10.1103/PhysRevD.90.075004. URL https://link.aps.org/doi/10.1103/PhysRevD.90.075004.

[5] J De Favereau, Christophe Delaere, Pavel Demin, Andrea Giammanco, Vincent Lemaitre, Alexandre Mertens, and Michele Selvaggi. Delphes 3: a modular framework for fast simulation of a generic collider experiment. *Journal of High Energy Physics*, 2014(2):1–26, 2014. URL https://arxiv.org/abs/1307.6346.

[6] Gabriella Gaudio. The idea detector concept for fcc-ee, 2022. URL https://pos.sissa.it/414/337/.

[7] Paolo Giacomelli. The idea detector concept, 2024. URL https://indico.mit.edu/event/876/contributions/2670/attachments/1034/1765/IDEA_detector-concept-FCC-US-2024.pdf.

[8] Andre Sailer. The cld detector concept, 2024. URL https://indico.mit.edu/event/876/contributions/2671/attachments/1037/1699/240325_sailer_cld.pdf.

[9] Matthew J. Strassler and Kathryn M. Zurek. Echoes of a hidden valley at hadron colliders. *Physics Letters B*, 651(5):374–379, 2007. ISSN 0370-2693. doi: https://doi.org/10.1016/j.physletb.2007.06.055. URL https://www.sciencedirect.com/science/article/pii/S0370269307007721.

[10] Taikan Suehara and Tomohiko Tanabe. Lcfiplus: A framework for jet analysis in linear collider studies. *Nuclear Instruments and Methods in Physics Research Section A: Accelerators, Spectrometers, Detectors and Associated Equipment*, 808:109–116, 2016. ISSN 0168-9002. doi: https://doi.org/10.1016/j.nima.2015.11.054. URL https://www.sciencedirect.com/science/article/pii/S0168900215014199.

[11] M. Tanabashi et al. Z boson pdg review, 2018. URL https://pdg.lbl.gov/2018/listings/rpp2018-list-z-boson.pdf.

[12] Ripellino Giulia Gonzalez Suarez Rebeca Vande Voorde, Magdalena. Long-lived particles from exotic higgs decays at the fcc-ee. URL https://repository.cern/records/3zatt-1vk66token=eyJhbGciOiJIUzUxMiJ9.eyJpZCI6ImMyMGFmN2M0LTA5NGEtNGZlNC05Y2FiLWVlMTIzZjQ3MGU0YSIsImRhdGEiOnt9LCJyYW5kb20iOiJlMGY 2foYqkj1F31QU7XF4UtpNF6EGFXibwec0_2DNlp7mgVsszYkAZPPjU0ehxsZYhnBSlbxll--JBwWebWVoI2LWQ.

[13] C. B. Verhaaren, J. Alimena, M. Bauer, P. Azzi, R. Ruiz, M. Neubert, O. Mikulenko, M. Ovchynnikov, M. Drewes, J. Klaric, A. Blondel, C. Rizzi, A. Sfyrla, T. Sharma, S. Kulkarni, A. Thamm, A. Blondel, R. Gonzalez Suarez, and L. Rygaard. Searches for long-lived particles at the future fcc-ee. *Frontiers in Physics*, 10, 2022. ISSN 2296-424X. doi: 10.3389/fphy.2022.967881. URL https://www.frontiersin.org/journals/physics/articles/10.3389/fphy.2022.967881.